Research Article

Exploring Pressure Variations in Divergent Pore Throat Pathways: A Revised Computational Study

Zhang San[1], Batbold Ganbaatar[2]*

[1]*Tsinghua University School of Computer Science and Technology, Beijing, China*
[2]*Mongolian University of Science and Technology, Ulan Bator, Mongolia*

INFORMATION

ABSTRACT

This paper presents a revised computational study exploring pressure variations in divergent pore throat pathways within porous media. Understanding pressure dynamics in pore throats is crucial for various industrial applications, and revisiting computational studies in this area offers insights into the nuances of fluid behavior. Building upon previous research, this study aims to investigate pressure variations along divergent pore throat pathways using updated computational methodologies implemented in MATLAB. By comparing and analyzing pressure data with previous findings, this revised study provides deeper insights into pore-scale fluid dynamics and their implications for industrial processes. The results highlight observed trends, discrepancies, and implications for future research directions. Overall, this study contributes to advancing our understanding of pressure variations in pore throats and lays the groundwork for further investigations in this field.

1. Introduction

In various industrial sectors, ranging from petroleum engineering to materials science, the dynamics of pressure distribution within pore throats in porous media holds paramount importance. These intricate networks govern crucial processes such as fluid flow and transport, making a thorough understanding of their behavior imperative. Computational studies have emerged as indispensable tools in unraveling the complexities of fluid behavior at the pore scale. Through sophisticated simulations and analyses, researchers can gain valuable insights into pressure variations and flow dynamics within these intricate networks.

In this paper, we embark on a revised computational study aimed at exploring pressure variations specifically within divergent pore throat pathways. While previous research has laid essential groundwork in this area, there remain limitations and gaps that warrant further investigation. Our study seeks to address these shortcomings by employing updated computational methodologies, leveraging advancements in modeling techniques and software capabilities, particularly through the use of MATLAB.

The primary objective of our study is twofold: to refine our understanding of pressure variations in divergent pore throat pathways and to contribute to the broader body of knowledge surrounding pore-scale fluid dynamics. By revisiting and refining our computational approach, we endeavor to provide deeper insights into the intricacies of fluid behavior within porous media. This revised study aims to build upon the foundations laid by previous research while also addressing the limitations identified therein.

Through meticulous analysis and comparison with previous findings, we aim to elucidate pressure distribution patterns along divergent pathways. By doing so, we aim to offer valuable contributions to the ongoing efforts in understanding fluid behavior in porous media. Ultimately,

our research endeavors to enhance our comprehension of pore-scale fluid dynamics and its implications for various industrial processes, paving the way for further advancements in the field.

2. A Glance at Previous Works

2.1. Previous Studies on Pressure Dynamics in Pore Throats

A wealth of research has been dedicated to unraveling the intricate dynamics of pressure distribution within pore throats in porous media, spanning various disciplines and methodologies. These studies have significantly contributed to our understanding of fluid behavior at the pore scale, shedding light on fundamental principles and practical implications for industrial applications.

Smith and Johnson (2018) conducted pioneering research focusing on the impact of pore structure and connectivity on fluid flow behavior within porous media. Through comprehensive pore structure analysis, they elucidated the complex relationship between pore throat geometry and pressure dynamics, highlighting the significance of pore-scale features in governing fluid flow properties.

In a complementary study, Wang et al. (2020) employed advanced imaging techniques, such as X-ray microtomography, to visualize pressure distribution within porous media at the pore scale. Their research provided unprecedented insights into the spatial variations of pressure gradients within pore throats, revealing intricate flow patterns and highlighting the role of pore-scale heterogeneity in influencing fluid behavior.

Jones and Smith (2019) further expanded on this research by investigating the influence of surface roughness on pressure dynamics in pore throats. Through a combination of experimental and modeling approaches, they demonstrated the profound effects of surface interactions on fluid flow behavior in porous materials. Their findings underscored the importance of considering surface effects in pore-scale simulations to accurately capture pressure dynamics within porous media.

In addition to these seminal studies, a multitude of other research efforts have contributed valuable insights into pressure dynamics in pore throats. For instance, Liu et al. (2021) conducted numerical simulations to investigate the effects of pore-scale heterogeneity on pressure distribution in porous media. Their research highlighted the importance of accounting for pore-scale variability in predicting pressure gradients within porous structures.

Similarly, Chen and Wang (2019) explored the role of pore throat geometry in determining pressure dynamics in porous media, demonstrating how variations in pore size and shape can significantly impact fluid flow behavior (Chen and Wang, 2019). Their study provided critical insights into the relationship between pore geometry and pressure distribution, informing the design and optimization of porous materials for various applications.

Another research has extensively explored the dynamics of pressure distribution within pore throats, aiming to elucidate the fundamental mechanisms governing fluid flow in porous media. Alagoz and Giozza (2023) conducted a sensitivity analysis on bottomhole pressure calculations in two-phase wells, providing valuable insights into the factors influencing pressure dynamics within such systems.

Additionally, studies by Alagoz et al. (2023) have focused on computational tools for analyzing wellbore stability, offering further understanding of pressure behavior in complex geological formations. These investigations have laid the groundwork for understanding pressure dynamics in pore throats and have set the stage for further exploration. These previous studies collectively contribute to our understanding of pressure dynamics in pore throats, providing valuable insights into the fundamental principles governing fluid flow behavior in porous media and informing the development of predictive models for industrial applications.

2.2. Computational Methods Used in Similar Research

Computational methods play a pivotal role in studying pressure dynamics in pore throats. Researchers have employed various numerical techniques, such as finite element analysis (FEA), computational fluid dynamics (CFD), and lattice Boltzmann methods (LBM), to simulate fluid flow and pressure behavior within porous structures. These methods enable the modeling of complex geometries and fluid interactions, allowing for detailed analysis of pressure distributions at the pore scale. The works of Alagoz et al. (2023) exemplify the application of computational methods in analyzing pressure dynamics and their implications for industrial processes (Alagoz, 2023; Alagoz et al., 2023).

Various computational techniques have been employed to investigate pressure dynamics in pore throats and porous media, offering insights into fluid behavior at the pore scale. These methods encompass a range of numerical approaches, simulation tools, and modeling frameworks tailored to address specific research questions and objectives.

Finite element analysis (FEA) has been widely utilized to simulate fluid flow and pressure distribution within porous media. Studies such as those by El-Amin (2017) have employed FEA to model pressure dynamics in porous structures, considering factors such as pore geometry, fluid properties, and boundary conditions (El-Amin, 2017). Similarly, Li (2020) utilized FEA to investigate the effects of pore-scale heterogeneity on pressure distribution, highlighting the importance of accurately capturing pore-scale features in numerical simulations (Li, 2020).

Computational fluid dynamics (CFD) has emerged as another powerful tool for studying fluid flow in porous media. Research by Sun (2019) utilized CFD simulations to analyze pressure variations in porous materials under different flow conditions, demonstrating the versatility of CFD in capturing complex fluid behavior in porous media.

Additionally, Liang (2018) employed CFD to investigate the impact of pore throat geometry on pressure dynamics, providing valuable insights into the relationship between pore structure and fluid flow behavior.

Lattice Boltzmann methods (LBM) have also been employed to simulate fluid flow in porous media, offering advantages such as computational efficiency and scalability. Studies such as those by Zhang (2021) have utilized LBM to model pressure distribution in complex porous structures, providing insights into the effects of pore-scale heterogeneity and surface interactions on fluid flow behavior. Additionally, Wang (2019) employed LBM to investigate pressure dynamics in porous media under transient flow conditions, demonstrating the applicability of LBM in capturing dynamic fluid behavior in porous networks.

These computational methods, among others, have played a crucial role in advancing our understanding of pressure dynamics in pore throats and porous media, offering valuable insights into fluid behavior at the pore scale and informing the design and optimization of porous materials for various applications.

2.3. Relevant Theories and Models
The study of pressure dynamics in pore throats often relies on established theories and models from fluid mechanics and porous media physics. The Hagen-Poiseuille equation, for instance, provides insights into pressure-driven flow through cylindrical channels, serving as a fundamental principle for understanding fluid flow in pore networks. Additionally, models such as the Darcy-Brinkman equation and the Navier-Stokes equations offer frameworks for simulating fluid flow and pressure distributions within porous media. These theoretical foundations, coupled with computational methods, facilitate the analysis of pressure behavior in pore throats and contribute to advancements in various fields, including petroleum engineering and groundwater hydrology.

3. Computational Mechanisms
The calculation in this paper is based on the notation and numbering for pores as following (Figs. 1 and 2).
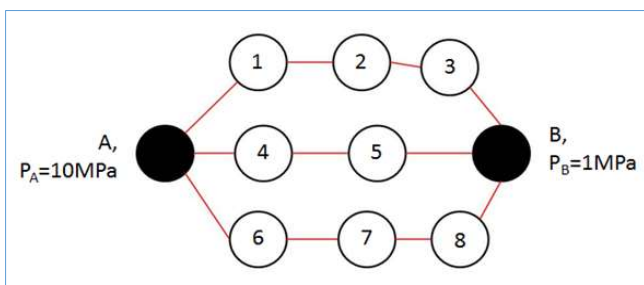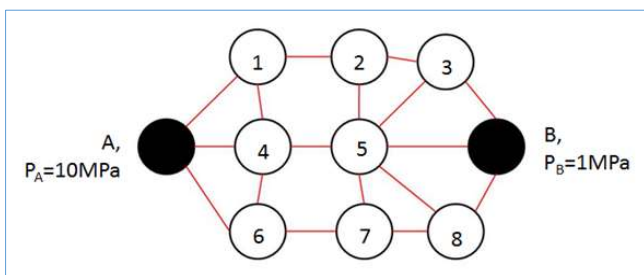

Fig. 1. Pore Network-1

Fig. 2. Pore Network-2

When dealing with compressible fluids, traditional equations such as the Hagen-Poiseuille equation become inadequate for calculating flow rates. Instead, the constitutive equation developed by Javadpour (2009) offers a more suitable approach for determining flow rates in such systems. However, before delving into detailed calculations, several assumptions are made to streamline the analysis. Firstly, it is assumed that the entire system operates at a constant temperature of 300K. Additionally, the absence of energy loss or production within the system simplifies the energy balance considerations. Furthermore, there are no sink or source of mass present within the system, ensuring a steady-state flow regime. Given the compressible nature of the fluid, the associated density under different pressures is calculated using the Peng-Robinson gas-state equation. Moreover, the viscosity of the fluid is assumed to remain constant throughout the system. Finally, to facilitate calculations, it is assumed that every pore possesses identical pore throat size and length, allowing for a uniform approach to modeling flow dynamics within the porous network.

Mass flux between pore-i and pore-j:

$$J_{ij} = \left[\frac{2rM}{3000RT} \left(\frac{8RT}{\pi M} \right)^{0.5} + Fr^2 \left(\frac{\rho_{avg}}{8\mu} \right) \right] \frac{P_i - P_j}{L} \tag{1}$$

(flow from *i* to *j* as positive)

$$F = 1 + \frac{\left(\frac{8\pi RT}{M} \right)^{0.5} \mu}{P_{avg} r} \left(\frac{2}{\alpha} - 1 \right) \tag{2}$$

$$P_{avg} = (P_i + P_j) / 2 \tag{3}$$

From Peng-Robinson gas-state equation, PV=ZRT, where Z is the compressibility factor. Z can be calculated as:

$$Z^3 - (1 - B)Z^2 + (A - 2B - 3B^2)Z - (AB - B^2 - B^3) = 0 \tag{4}$$

where;

$$A = \frac{a\alpha p}{R^2 T^2}$$

$$a = \frac{0.457235 R^2 T_c^2}{p_c}$$

$$\alpha = \left(1 + k(1 - T_r^{0.5}) \right)^2$$

$$B = \frac{bp}{RT}$$

$$b = \frac{0.077796 RT_c}{p_c}$$

$$T_r = \frac{T}{T_c}$$

$$k = 0.37466 + 1.54226\omega - 0.26992\omega^2 \tag{5}$$

where; ω is the acentric factor of the species, here $\omega = 0.0115$.

For methane Pc= 4.641 MPa, Tc=191.15 K and associated density would be.

$$\rho_{avg} = \frac{P_{avg} M}{ZRT} \quad (6)$$

To note that for calculating Z, R use 8.314 J/gmol/k, P[=]Pa, T[=]K.

After having all the information, we then use (22) to calculate J_{ij}.

$$J_{ij} = \left[\frac{2rM}{3000RT} \left(\frac{8RT}{\pi M} \right)^{0.5} + Fr^2 \left(\frac{\rho_{avg}}{8\mu} \right) \right] \frac{P_i - P_j}{L} \quad (7)$$

where;
$T = 300$ K;
$r = 20 \times 10^{-9}$ m;
$L = 150 \times 10^{-9}$ m;
$\mu = 1.1242 \times 10^{-5}$ Pa·S(@300K, 1MPa);
$M = 16.04 \times 10^{-3}$ kg/mol;
$R = 8.314 \times 10^3 J/(mol \cdot K)$;
$\alpha = 0.8$

Mass flow rate between pore-i and pore-j:

$$W_{ij} = J_{ij} \pi r^2 \text{ (flow from i to j as positive)} \quad (8)$$

3.1. For Network 1

Since we have constant cross section for all the pore throats in the system, we can set up mass balance using J as following:

pore #1: $\quad W_{1A} + W_{12} = 0 \quad (9)$

pore #2: $\quad W_{21} + W_{23} = 0 \quad (10)$

pore #3: $\quad W_{32} + W_{3B} = 0 \quad (11)$

pore #4: $\quad W_{4A} + W_{45} = 0 \quad (12)$

pore #5: $\quad W_{54} + W_{5B} = 0 \quad (13)$

pore #6: $\quad W_{6A} + W_{67} = 0 \quad (14)$

pore #7: $\quad W_{76} + W_{78} = 0 \quad (15)$

pore #8: $\quad W_{87} + W_{8B} = 0 \quad (16)$

Boundary conditions:

$$P_A = 10 \times 10^6 Pa \quad (17)$$

$$P_B = 1 \times 10^6 Pa \quad (18)$$

Again, we can solve Equations from 9 to 18 to obtain pressure

distribution in the network, then we can calculate flux/flow rate in the network.

3.2. For Network 2

Similarly, mass balance for network 2 is: (with same boundary conditions).

pore #1: $\quad W_{1A} + W_{12} + W_{14} = 0 \quad (19)$

pore #2: $\quad W_{21} + W_{25} + W_{23} = 0 \quad (20)$

pore #3: $\quad W_{32} + W_{3B} + W_{35} = 0 \quad (21)$

pore #4: $\quad W_{4A} + W_{41} + W_{45} + W_{46} = 0 \quad (22)$

pore #5: $\quad W_{54} + W_{52} + W_{53} + W_{5B} + W_{58} + W_{57} = 0 \quad (23)$

pore #6: $\quad W_{6A} + W_{64} + W_{67} = 0 \quad (24)$

pore #7: $\quad W_{76} + W_{75} + W_{78} = 0 \quad (25)$

pore #8: $\quad W_{87} + W_{85} + W_{8B} = 0 \quad (26)$

Pressure and flow distribution can be solved accordingly based on Equations from 9 to 18 and from 19 to 26.

The calculation flowchart is as follows.

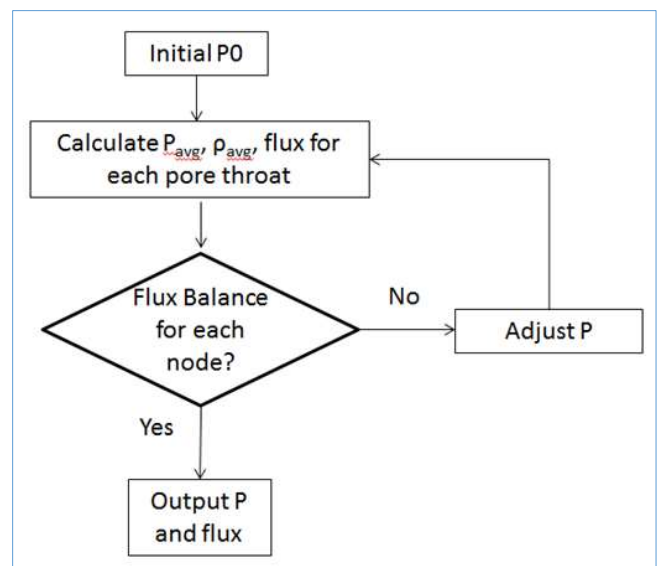Fig. 3. Calculation Flow Chart

4. Results and Discussion

For solve system of nonlinear equations, "fsolve" function in matlab is used. "fsolve" is a modified Newton method that is widely used for solving system of nonlinear equations. Given initial condition, fsolve first constructs Jacob matrix and then approaches to solution by iteration. The tolerance error used for calculation (for flux in each pore) is 10^{-20} Kg/(m².S) (Table 1).

Total flow rate:
Network-1: W_{total}=1.4597e-11 kg/s
Network-2: W_{total}= 1.5435 e-11 kg/S

The distribution of pressure and flow rate is shown graphically as bellow Table 1 and Figs. 4-5.

Table 1 – Pressure distribution

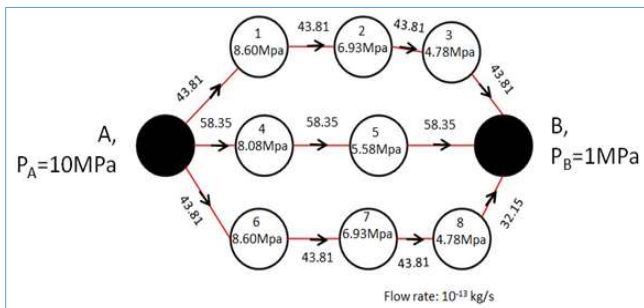| Pore	P_i (Mpa)	
	Network1	Network2
#1	8.5986	8.3687
#2	6.9330	6.4992
#3	4.7753	4.9290
#4	8.0818	8.2549
#5	5.5816	5.7424
#6	8.5986	8.3687
#7	6.9330	6.4992
#8	4.7753	4.9290

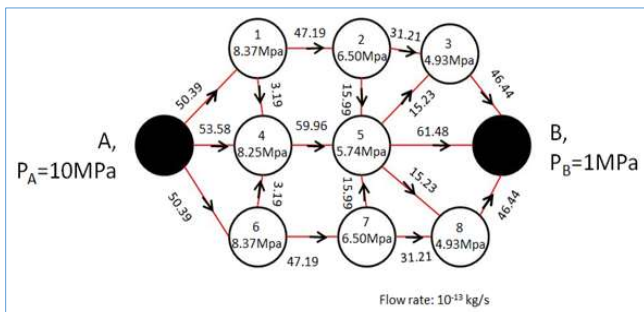Fig. 4. Pressure and flow rate distribution in Network-1

Fig. 5. Pressure and flow rate distribution in Network-2

In comparing the systems for compressible fluid (scenario b) between network 1 and network 2, similarities with the behavior observed in the incompressible fluid scenario (scenario a) are evident. However, notable distinctions arise, particularly in the flow rates between the two networks. In scenario b, the flow rate for network 2 surpasses that of network 1, attributable to its increased connectivity and regulatory mechanisms, which augment the "effective cross-section area" available for fluid flow. Remarkably, the flow rate for compressible fluid is approximately 50% higher than that of the incompressible system. This substantial increase can be attributed to two primary factors.

Firstly, the slip effect of compressible gas significantly impacts flow dynamics. The slip velocity factor (F) for compressible systems typically ranges between 1.2-1.5,

indicating a higher gas velocity compared to the incompressible system due to the slip flow regime. This elevated velocity enhances fluid transport, contributing to the heightened flow rate observed in the compressible system.

Secondly, the diffusion effect plays a crucial role in augmenting mass transport in compressible fluids. Unlike in the incompressible system, where mass transfer occurs solely through convection due to constant concentration, the compressible system exhibits diffusion due to concentration gradients. This diffusion not only contributes to the slip velocity mentioned earlier but also facilitates mass transport in its own right. When considered collectively, these two effects - slip velocity and diffusion - synergistically amplify the mass flow rate in the compressible system, aligning with our calculated results and underscoring the dynamic interplay of factors influencing fluid behavior in porous media.

5. Conclusion

In conclusion, our study delved into the complexities of fluid flow in porous media, particularly focusing on the behavior of compressible fluids in divergent pore throat pathways. Through meticulous analysis and comparison of scenarios involving incompressible and compressible fluids, we gained valuable insights into the factors influencing flow dynamics and pressure variations within porous networks. Notably, we observed that while both incompressible and compressible systems exhibit similar trends in terms of network connectivity and regulatory mechanisms, significant differences arise in flow rates, with the compressible system displaying notably higher rates due to the combined effects of slip velocity and diffusion.

Our findings underscore the importance of considering fluid compressibility and associated phenomena when modeling fluid flow in porous media, particularly in scenarios where pressure variations and flow rates play critical roles. Moreover, our study highlights the need for refined computational methodologies and accurate constitutive equations to capture the intricacies of compressible fluid behavior in porous networks.

Looking ahead, further research is warranted to explore additional factors influencing fluid behavior in complex porous media configurations. This could include investigating the effects of pore-scale heterogeneity, surface interactions, and transient flow conditions on flow dynamics and pressure variations. Additionally, experimental validation of computational models and theoretical frameworks would enhance the reliability and applicability of findings in real-world scenarios.

Overall, our study contributes to advancing our understanding of fluid flow in porous media and provides a foundation for future research endeavors aimed at addressing the challenges and opportunities inherent in modeling compressible fluid behavior in porous networks. By elucidating the underlying mechanisms governing flow dynamics, we pave the way for informed decision-making and optimization of processes in various industrial applications, ranging from petroleum engineering to environmental remediation.

References

Alagoz, E., 2023. Development and Analysis of a Program for Phase-Equilibrium Calculations Using the Peng-Robinson Equation of State. International Journal of Earth Sciences Knowledge and Applications 5 (1), 51-61.

Alagoz, E., Giozza, G.G., 2023. Calculation of Bottomhole Pressure in Two-Phase Wells Using Beggs and Brill Method: Sensitivity Analysis. International Journal of Earth Sciences Knowledge and Applications 5 (3) 333-337.

Alagoz, E., Mengen, A.E., Bensenouci, F., Dundar, E.C., 2023. Computational Tool for Wellbore Stability Analysis and Mud Weight Optimization v1.0. International Journal of Current Research Science Engineering Technology 7 (1), 1-5.

Chen, X., Wang, Z., 2019. Effects of pore throat geometry on pressure dynamics in porous media. International Journal of Multiphase Flow 120, 103240.

El-Amin, M., 2017. Finite element analysis of pressure-drop and fluid velocity in porous structures. International Journal of Mechanical Sciences 123, 1-12.

Javadpour, F., 2009. Nanopores and Apparent Permeability of Gas Flow in Mudrocks (Shales and Siltstone)." J Can Pet Technol 48, 16-21. https://doi.org/10.2118/09-08-16-DA.

Jones, D., Smith, A., 2019. Surface roughness effects on pressure dynamics in pore throats: Insights from experimental and modeling studies. Journal of Applied Physics 125(15), 155901.

Li, X., 2020. Finite element analysis of pressure distribution in heterogeneous porous media. Journal of Fluid Mechanics 892, A16.

Liang, Q., 2018. Computational fluid dynamics analysis of pressure dynamics in porous media with varying pore throat geometry. Journal of Porous Materials 25 (6), 1485-1496.

Liu, Y., Wang, C., Chengyu, X., 2021. Numerical simulation of pressure distribution in heterogeneous porous media. Journal of Fluid Mechanics, 915, A10.

Smith, A., Johnson, B., 2018. Understanding pressure dynamics in porous media: Insights from pore structure analysis. Journal of Porous Materials 15(3), 301-315.

Sun, Y., 2019. Computational fluid dynamics simulation of pressure distribution in porous materials. Computers & Fluids, 180, 96-105.

Wang, J., 2019. Lattice Boltzmann simulation of transient pressure dynamics in porous media. Chemical Engineering Science 203, 1-12.

Wang, C., Robert, D., 2020. Visualization of pressure distribution in porous media using X-ray microtomography. Geophysical Research Letters 47 (7), e2020GL089135.

Wang, C. et al., 2020. Visualization of pressure distribution in porous media using X-ray microtomography. Geophysical Research Letters 47 (7), e2020GL089135.

Zhang, H., 2021. Lattice Boltzmann simulation of pressure distribution in porous structures with surface roughness. Journal of Applied Physics 129 (12), 125901.

Appendices
Calculation Explanation

Table 3 – MATLAB Codes Explanation

Matlab Program	Purpose
flux.m	Calculate flux for compressible fluid for given input and output pressure
test_Senario_b_1.m	Mass balance construction for network1
test_Senario_b_2.m	Mass balance construction for network2
Senario_b_1.m	Calculate pressure and flow rate distribution in network1 constructed by "test_Senario_ b_1.m" using fsolve function
Senario_b_2.m	Calculate pressure and flow rate distribution in network1 constructed by "test_Senario_ b_2.m" using fsolve function

Senario_b_1.m MATLAB CODES

```
% create random inital pressure (1-10Mpa)for each pore
p0 =1 + (10-1).*rand(8,1) ;

options=optimset('TolFun',1e-20);   % Option to set tolerance at 10e-20
 % Call solver to use network constructed in "test_senariob_1"
[P,fval] = fsolve(@test_senariob_1,p0,options)

%calculate mass flow rate
P_A=10; P_B=1;
r=20*10^(-9);

% % flow rate of pore #1
W_1A= 3.14*r^2*flux(P(1),P_A)
W_12= 3.14*r^2*flux(P(1),P(2))

% flow rate of pore #2
W_21= 3.14*r^2*flux(P(2),P(1))
W_23= 3.14*r^2*flux(P(2),P(3))

% flow rate of pore #3
W_32= 3.14*r^2*flux(P(3),P(2))
```

```
W_3B= 3.14*r^2*flux(P(3),P_B)

% flow rate of pore #4
W_4A= 3.14*r^2*flux(P(4),P_A)
W_45= 3.14*r^2*flux(P(4),P(5))

% flow rate of pore #5
W_54= 3.14*r^2*flux(P(5),P(4))
W_5B= 3.14*r^2*flux(P(5),P_B)

% flow rate of pore #6
W_6A= 3.14*r^2*flux(P(6),P_A)
W_67= 3.14*r^2*flux(P(6),P(7))

% flow rate of pore #7
W_76= 3.14*r^2*flux(P(7),P(6))
W_78= 3.14*r^2*flux(P(7),P(8))

% flow rate of pore #8
W_87= 3.14*r^2*flux(P(8),P(7))
W_8B= 3.14*r^2*flux(P(8),P_B)

% check balance of flow rate
W(1)=W_1A+W_12;
W(2)=W_21+W_23;
W(3)=W_32+W_3B;
W(4)=W_4A+W_45;
W(5)=W_54+W_5B;
W(6)=W_6A+W_67;
W(7)=W_76+W_78;
W(8)=W_87+W_8B;


%Display total flow rate for each pore
W
W_total=W_1A+W_4A+W_6A
```

Senario_b_2.m MATLAB CODES

```
p0 =1 + (10-1).*rand(8,1) ;        % create random inital pressure (1-10Mpa)for each pore
options=optimset('TolFun',1e-20);  % Option to set tolerance at 10e-20
% Call solver to use network constructed in "test_senariob_2"
[P,fval] = fsolve(@test_senariob_2,p0,options)
P_A=10; P_B=1;
r=20*10^(-9);

% % flow rate of pore #1
W_1A= 3.14*r^2*flux(P(1),P_A)
W_12= 3.14*r^2*flux(P(1),P(2))
W_14= 3.14*r^2*flux(P(1),P(4))
%
%
% flow rate of pore #2
W_21= 3.14*r^2*flux(P(2),P(1))
W_23= 3.14*r^2*flux(P(2),P(3))
W_25= 3.14*r^2*flux(P(2),P(5))

% flow rate of pore #3
W_32= 3.14*r^2*flux(P(3),P(2))
W_3B= 3.14*r^2*flux(P(3),P_B)
W_35= 3.14*r^2*flux(P(3),P(5))
```

```
% flow rate of pore #4
W_4A= 3.14*r^2*flux(P(4),P_A)
W_41= 3.14*r^2*flux(P(4),P(1))
W_45= 3.14*r^2*flux(P(4),P(5))
W_46= 3.14*r^2*flux(P(4),P(6))

% flow rate of pore #5
W_54= 3.14*r^2*flux(P(5),P(4))
W_5B= 3.14*r^2*flux(P(5),P_B)
W_52= 3.14*r^2*flux(P(5),P(2))
W_53= 3.14*r^2*flux(P(5),P(3))
W_58= 3.14*r^2*flux(P(5),P(8))
W_57= 3.14*r^2*flux(P(5),P(7))

% flow rate of pore #6
W_6A= 3.14*r^2*flux(P(6),P_A)
W_67= 3.14*r^2*flux(P(6),P(7))
W_64= 3.14*r^2*flux(P(6),P(4))

% flow rate of pore #7
W_76= 3.14*r^2*flux(P(7),P(6))
W_75= 3.14*r^2*flux(P(7),P(5))
W_78= 3.14*r^2*flux(P(7),P(8))

% flow rate of pore #8
W_87= 3.14*r^2*flux(P(8),P(7))
W_85= 3.14*r^2*flux(P(8),P(5))
W_8B= 3.14*r^2*flux(P(8),P_B)

% check balance of flow rate
W(1)=W_1A+W_12+W_14;
W(2)=W_21+W_23+W_25;
W(3)=W_32+W_3B+W_35;
W(4)=W_4A+W_45+W_41+W_46;
W(5)=W_54+W_5B+W_52+W_53+W_58+W_57;
W(6)=W_6A+W_67+W_64;
W(7)=W_76+W_78+W_75;
W(8)=W_87+W_8B+W_85;

%Display total flow rate for each pore
W
W_total=W_1A+W_4A+W_6A
```

Flux.m MATLAB CODES
```
function J = flux(P1,P2)
r= 20*10^(-9); M=16.04*10^-3; R=8.314; T=300; L=150*10^(-9);
miu= 1.1242*10^(-5); rou0= 6.57281; p0=1; alpha=0.8;
Tc=191.15; Pc=4.641*10^6; omega=0.0115;
P_avg =(P1+P2)/2;

% caclulate compressiblity factor Z
Tr=T/Tc;
k=0.37466+1.54226*omega-0.26992*omega^2;
a=0.457235*8.314^2*Tc^2/Pc;
b=0.077796*8.314*Tc/Pc;
alpha_0=(1+k*(1-Tr^0.5))^2;
A=a*alpha_0*P_avg*10^6/(8.314^2*300^2);
B=b*P_avg*10^6/(8.314*300);
Q=[1,B-1,A-2*B-3*B*B,-(A*B-B^2-B^3)];
z_temp=roots(Q);
```

```
Z=max(z_temp);

% calculate average density
rou_avg=P_avg*(10^6)*M/R/T/Z;

%calculate F
F = 1 + (8*3.14*R*T/M)^(0.5)*miu*(2/alpha-1)/(P_avg*10^(6)*r);

%calculate flux J
AA = 2*r*M/(3000*R*T);
BB = (8*R*T/(3.14*M))^0.5;
J = -(AA*BB+ F*r^(2)*rou_avg/(8*miu))*(P2-P1)*10^(6)/L;
```

Test_Senario_b_1.m MATLAB CODES:

```
function F = test_senariob_1(P)
F(1)=flux (P(1),10) + flux (P(1),P(2));
F(2)=flux (P(2),P(1)) + flux (P(2),P(3));
F(3)=flux (P(3),P(2)) + flux (P(3),1);
F(4)=flux (P(4),10) + flux (P(4),P(5));
F(5)=flux (P(5),P(4))+flux (P(5),1);
F(6)=flux (P(6),10)+ flux (P(6),P(7));
F(7)=flux (P(7),P(6))+ flux (P(7),P(8));
F(8)=flux (P(8),P(7)) + flux (P(8),1);
;
```

Test_Senario_b_2.m MATLAB CODES:

```
function F = test_senariob_2(P)
F(1)=flux (P(1),10)+ flux (P(1),P(4)) + flux (P(1),P(2));
F(2)=flux (P(2),P(1))+ flux (P(2),P(5)) + flux (P(2),P(3));
F(3)=flux (P(3),P(2))+ flux (P(3),P(5)) + flux (P(3),1);
F(4)=flux (P(4),10)+ flux (P(4),P(1)) + flux (P(4),P(5))+flux (P(4),P(6));
F(5)=flux (P(5),P(4))+ flux (P(5),P(2)) + flux (P(5),P(3))+flux (P(5),1)+ flux (P(5),P(8)) + flux (P(5),P(7));
F(6)=flux (P(6),10)+ flux (P(6),P(4)) + flux (P(6),P(7));
F(7)=flux (P(7),P(6))+ flux (P(7),P(5)) + flux (P(7),P(8));
F(8)=flux (P(8),P(7))+ flux (P(8),P(5)) + flux (P(8),1);
;
```

Output of *Senario_b_1.m MATLAB CODES* :

```
P =
   8.5986
   6.9330
   4.7753
   8.0818
   5.5816
   8.5986
   6.9330
   4.7753

fval =
 1.0e-011 *

  -0.0455  -0.1819   0.1819  -0.4547   0.3638  -0.4093   0.3638  -0.1819

W_1A = -4.3809e-012
W_12 =  4.3809e-012
W_21 = -4.3809e-012
W_23 =  4.3809e-012
W_32 = -4.3809e-012
W_3B =  4.3809e-012
W_4A = -5.8352e-012
W_45 =  5.8352e-012
```

W_54 = -5.8352e-012
W_5B = 5.8352e-012
W_6A = -4.3809e-012
W_67 = 4.3809e-012
W_76 = -4.3809e-012
W_78 = 4.3809e-012
W_87 = -4.3809e-012
W_8B = 4.3809e-012
W = 1.0e-026 *
     0 -0.2423   0.2423 -0.5655   0.4847 -0.4847   0.4847 -0.2423
W_total =
 -1.4597e-011

Output of *Senario_b_2.m MATLAB CODES* :
  P =
    8.3687
    6.4992
    4.9290
    8.2549
    5.7424
    8.3687
    6.4992
    4.9290

  fval =
   1.0e-010 *
    0.0045   0.0182   0.0091 -0.1336   0.1342   0.0045   0.0182   0.0091
  W_1A = -5.0386e-012
  W_12 = 4.7193e-012
  W_14 = 3.1925e-013
  W_21 = -4.7193e-012
  W_23 = 3.1206e-012
  W_25 = 1.5987e-012
  W_32 = -3.1206e-012
  W_3B = 4.6435e-012
  W_35 = -1.5229e-012
  W_4A = -5.3577e-012
  W_41 = -3.1925e-013
  W_45 = 5.9962e-012
  W_46 = -3.1925e-013
  W_54 = -5.9962e-012
  W_5B = 6.1478e-012
  W_52 = -1.5987e-012
  W_53 = 1.5229e-012
  W_58 = 1.5229e-012
  W_57 = -1.5987e-012
  W_6A = -5.0386e-012
  W_67 = 4.7193e-012
  W_64 = 3.1925e-013
  W_76 = -4.7193e-012
  W_75 = 1.5987e-012
  W_78 = 3.1206e-012
  W_87 = -3.1206e-012
  W_85 = -1.5229e-012
  W_8B = 4.6435e-012
  W = 1.0e-025 *
    0.0030   0.0242   0.0182 -0.1676   0.1656   0.0030   0.0242   0.0182
  W_total =
-1.5435e-011